Results from deep inelastic scattering at HERA

J. J. Whitmore (on behalf of the ZEUS and H1 Collaborations) [a*]

[a]Department of Physics, Penn State University,
University Park, PA 16802, USA

Recent results from the ZEUS and H1 collaborations at HERA on the structure of the proton are reviewed. The emphasis is on the quark and gluon distributions as well as electroweak effects at high Q^2.

1. INTRODUCTION

Since 1994, the ZEUS and H1 experiments have accumulated 48 and 37 pb^{-1}, respectively, of e^+p data with a proton energy of 820 GeV. In the 1998-99 running periods, they have collected 13 and 14 pb^{-1}, respectively, of e^-p data with 920 GeV protons.

For the discussion of deep inelastic scattering (DIS), the standard variables are: $Q^2 = -q^2 = -(k-k')^2 = 2E_eE'_e(1-\cos\theta)$, the negative of the four-momentum transfer squared ($-$mass^2 of the virtual photon); $x = \frac{Q^2}{2P\cdot q} = \frac{Q^2}{sy}$, the momentum fraction of the struck parton in the proton ($0 < x < 1$); $y = \frac{P\cdot q}{P\cdot k} = 1 - \frac{E'_e}{2E_e}(1+\cos\theta)$, the fractional energy transfer to the proton in its rest frame ($0 < y < 1$); and $W^2 = (P+q)^2 = \frac{Q^2(1-x)}{x} + m_p^2$, the square of the photon-proton center-of-mass energy (mass^2 of the hadronic system).

At HERA, the ep center-of-mass energy $\sqrt{s}$ is 300 (320) GeV for 27.5 GeV leptons on 820 (920) GeV protons. For the different regions in the kinematic plane, as $y \to 1$ the cross section is sensitive to effects of F_L, the longitudinal structure function; as $y \to 0.005$ there is an overlap with fixed-target experiments; at low Q^2, the transition from γ^*p to γp can be studied; at medium Q^2, various tests of pQCD can be made and at high Q^2, electroweak studies can be performed and searches for new physics are carried out.

2. NEUTRAL AND CHARGED CURRENT PROCESSES

2.1. Neutral current scattering

The differential cross section for the Neutral Current (NC) process $e^\pm p \to e^\pm X$ can be written in terms of the proton structure functions $F_2^{NC} = F_2^{\rm em} + \left(\frac{Q^2}{Q^2+M_Z^2}\right) F_2^{\rm int} + \left(\frac{Q^2}{Q^2+M_Z^2}\right)^2 F_2^{\rm weak}$ in terms of the γ and Z exchange contributions with $F_2^{em}(x,Q^2) = \sum_q x\, e_q^2\, [q(x,Q^2) + \bar{q}(x,Q^2)]$ + corrections in higher order QCD; $F_L^{NC}(x,Q^2)$, the longitudinal structure function, which is zero at leading order (LO), and $xF_3^{NC}(x,Q^2)$ the parity

*Work supported in part by the U.S. National Science Foundation and by the U.S.-Israel Binational Science Foundation.

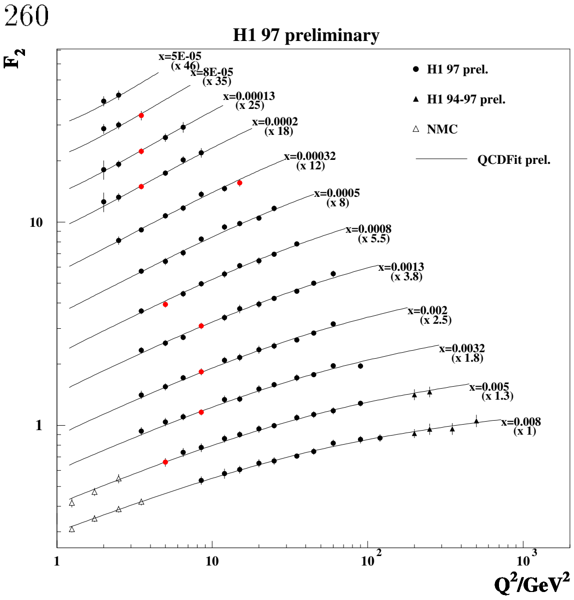

Figure 1. Preliminary measurements of F_2 as a function of Q^2 at fixed values of x.

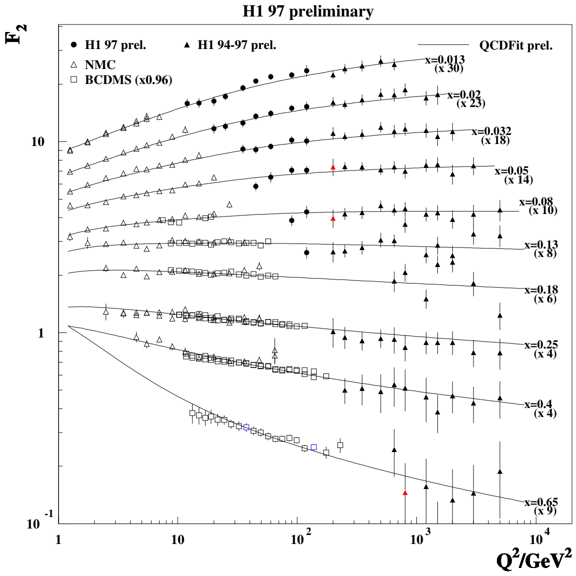

Figure 2. Preliminary measurements of F_2 as a function of Q^2 at fixed values of x.

violating term which is negligible for $Q^2 \ll M_Z^2$:

$$\frac{d^2\sigma(NC)}{dx\,dQ^2} = \frac{2\pi\alpha^2}{xQ^4}\left(Y_+F_2^{NC} - y^2F_L^{NC} \mp Y_-xF_3^{NC}\right) \quad (1)$$

where $Y_\pm = 1 \pm (1-y)^2$, In the LO approximation and neglecting Z exchange, the cross section can be expressed in terms of the quark parton distribution functions (pdf) as:

$$\frac{d^2\sigma^{LO}(e^+p)}{dx\,dQ^2} = \frac{2\pi\alpha^2}{xQ^4}Y_+\left(\frac{4}{9}x(u+\bar{u}+c+\bar{c}) + \frac{1}{9}x(d+\bar{d}+s+\bar{s})\right). \quad (2)$$

Figures 1 and 2 present an overview of the most recent measurements [1] of F_2. At small x, F_2 rises with Q^2 and displays the well-known scaling violations which are driven by the large gluon density, $xg(x,Q^2)$, with the DGLAP splitting function P_{qg}: $dF_2/dlnQ^2 \sim \alpha_s P_{qg} \otimes xg(x,Q^2)$. At $x \sim 0.1$, the cross section becomes independent of Q^2, i.e. scale invariance is exhibited. At higher x, F_2 falls with increasing Q^2. Note that the NLO QCD fit describes the data over 4 orders of magnitude in both Q^2 and x and that there is excellent agreement between the fixed-target and HERA data.

Figure 3 shows the ratio $\frac{\sigma(e^-p)}{\sigma(e^+p)}$ for the NC data [2]: at high Q^2, $e^-p > e^+p$, displaying the negative $\gamma - Z$ interference effects in e^+p and positive effects in e^-p. Similarly, Fig. 4 shows $d\sigma/dx$ for the e^-p and e^+p data [2]. The various curves show that the data are consistent with the Standard Model (SM) expectations of a Z with a mass of 91 GeV. The NLO QCD fits to the lower Q^2 data describe these high-Q^2 data well. These HERA NC data thus show clear evidence for Z-exchange in the $space-like$ region for DIS.

2.2. Charged current scattering

The differential cross section for the Charged Current (CC) process $e^\pm p \to \nu X$ is

$$\frac{d^2\sigma(CC)}{dx\,dQ^2} = \frac{G_F^2}{4\pi x}\left(\frac{M_W^2}{M_W^2+Q^2}\right)^2\left(Y_+F_2^{CC} - y^2F_L^{CC} \mp Y_-xF_3^{CC}\right), \quad (3)$$

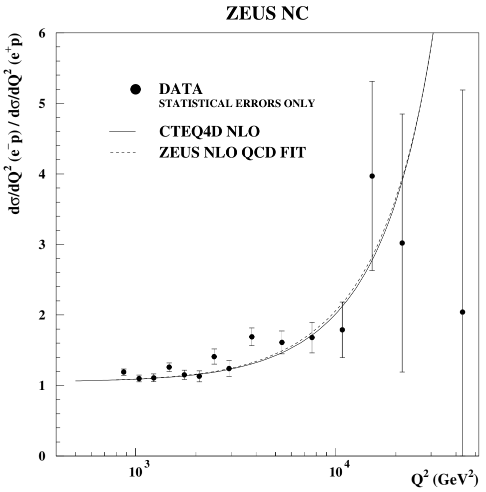

Figure 3. The ratio of the $e^{-}p$ cross section for $E_p = 920$ GeV to the $e^{+}p$ cross section for $E_p = 820$ GeV. The SM predictions are shown as the curves.

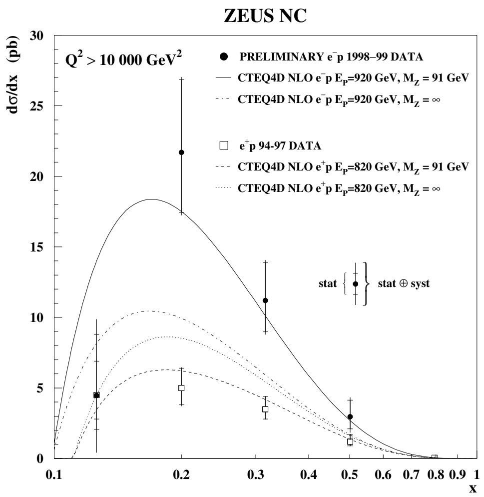

Figure 4. The differential cross section $d\sigma/dx$ for $Q^2 > 10000$ GeV^2. The solid (dashed) line shows the SM prediction for $e^{-}p$ ($e^{+}p$) scattering. The dot-dashed (dotted) line shows the calculation in which the Z contribution is ignored.

where G_F = Fermi Coupling Constant. This reduces in the LO approximation to

$$\frac{d^2\sigma^{LO}(e^+p)}{dx\,dQ^2} = \frac{G_F^2}{2\pi x}\left(\frac{M_W^2}{M_W^2+Q^2}\right)^2\Big[x(\bar{u}+\bar{c})+(1-y)^2x(d+s)\Big]. \tag{4}$$

Figure 5 presents the recent CC measurements of $d\sigma/dQ^2$ for both $e^{+}p$ and $e^{-}p$ [3]. Equation (4) shows that $d\sigma/dQ^2(e^-p) \sim xu$ while $d\sigma/dQ^2(e^+p) \sim (1-y)^2xd$. The ratio $\frac{\sigma(e^-p)}{\sigma(e^+p)}$ for CC is shown in the lower plot. This ratio is ~ 10 at high Q^2 and both the cross section and the ratio are in excellent agreement (see curves) with the SM for over 5 orders of magnitude in the cross section.

Figure 6 shows the reduced cross section (for which the propagator effects are diminished so the pdf's are more visible) defined, for $e^{+}p$, as

$$\tilde{\sigma} = \frac{2\pi x}{G_F^2}\frac{(Q^2+M_W^2)^2}{M_W^4}\frac{d^2\sigma^{CC}}{dxdQ^2} = x\Big[(\bar{u}+\bar{c})+(1-y)^2(d+s)\Big] \tag{5}$$

as a function of x for different values of Q^2 [4]. The curves show that at high Q^2, $\tilde{\sigma}$ dominated by the d-quark contribution, that there is good agreement with the SM using the pdf's from CTEQ4D and from low Q^2 fits and that these data can be used to constrain the particular parton flavors for the proton structure. These data have also been used [5] to determine the mass of the W-boson from the propagator shape: $\frac{d\sigma^{CC}}{dQ^2} \propto G_F^2 \cdot \left[\frac{M_W^2}{Q^2+M_W^2}\right]^2$. Here also, the cross section shows the effects of the W boson in the $space-like$ regime.

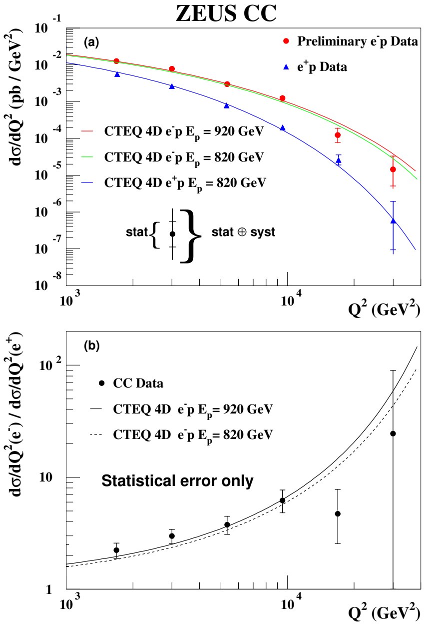

Figure 5. (Upper) Comparison of the differential cross sections $d\sigma/dQ^2$ for e^+p and e^-p DIS; (lower) the ratio of the cross sections. The SM predictions are shown as the curves.

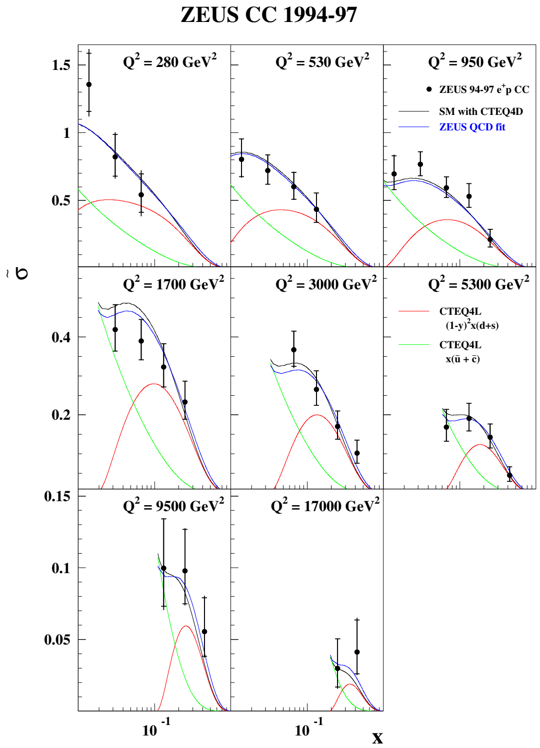

Figure 6. The reduced cross section σ_r as a function of x for fixed values of Q^2. The LO $x(\bar{u}+\bar{c})$ and $(1-y)^2x(d+s)$ are shown as the dotted and dashed lines, respectively.

3. MEASUREMENT OF F_2^c

This semi-inclusive structure function measurement requires the observation of open charm in the hadronic final state:

$$\frac{d^2\sigma(ep \to ec\bar{c}X)}{dx\, dQ^2} = \frac{2\pi\alpha^2}{xQ^4}\left(Y_+F_2^c - y^2F_L^c\right). \tag{6}$$

Both H1 [6] and ZEUS [7] measure F_2^c from events with tagged charm, e.g. $D^{*\pm} \to D^0\pi^\pm_{\rm slow}$ with $D^0 \to K\pi$ or $K3\pi$. It has been found that charm is generated predominantly by the boson-gluon fusion (BGF) process: $\gamma g \to c\bar{c}$. Figure 7 shows the resulting $D^*(2010)$ cross section [7] as a function of different kinematic variables. The shaded bands are the result of a calculation based on NLO BGF (HVQDIS, Harris and Smith [8]) for $c\bar{c}$ production. This calculation uses the fragmentation function $c \to D^*$ (0.222 from OPAL), the branching ratio for $D^{*\pm} \to D^0\pi_s^\pm$ (68.3%, PDG) and the gluon distribution obtained from NLO QCD fits to the scaling violations of F_2. The good agreement demonstrates the universality of the gluon. If the cross sections are extrapolated to all phase space using NLO to get F_2^c, one observes strong scaling violations, indicative of the rising gluon at small x. In fact, the rise of F_2^c is stronger [7] than that of F_2 and the charm content of the proton rises (with Q^2) from $\approx 10\%$ at 1.8 GeV^2 to $\approx 25\%$ at 130 GeV^2 [9].

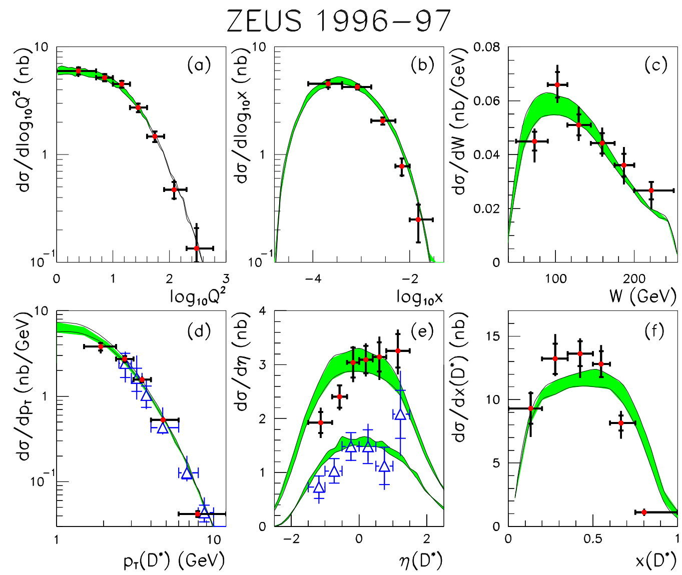

Figure 7. Differential cross sections for $D^*(2010)$ production as a function of (a) Q^2, (b) x, (c) W, (d) $p_T(D^*)$, (e) $\eta(D^*)$ and (f) $x(D^*)$. The bands correspond to the HVQDIS result with $m_c = 1.3$ (upper) and 1.5 GeV (lower).

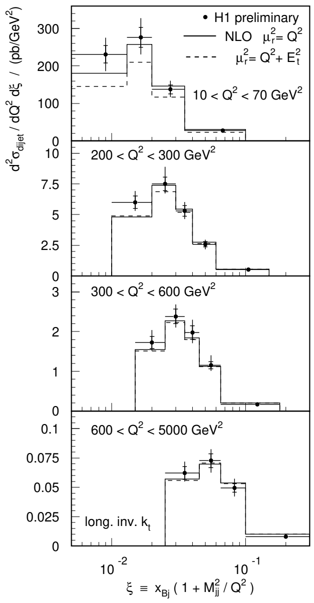

Figure 8. DIS dijet cross section as a function of Q^2 and $\xi = x_{Bj}(1 + M_{jj}^2/Q^2)$. The data are compared to the NLO calculation with two different renormalization scales.

4. JETS IN DEEP INELASTIC SCATTERING

Yet another method to study the gluon distribution is via the study of DIS jets analysed in the Breit frame. Figure 8 shows the measured cross section [10] compared to a NLO calculation based on the BGF process for two different renormalization schemes in which $\mu_r^2 = Q^2 + E_T^2$ or Q^2. From a NLO QCD fit to the cross section (with quark densities determined from F_2 data), H1 find a gluon distribution which is consistent with that found in F_2 (scaling violations) and F_2^c.

5. DIFFRACTION

Inclusive diffraction at HERA corresponds to the diffractive excitation of the virtual γ into a system with the same quantum numbers as the photon, while the final baryonic system has the same quantum numbers as the initial proton. This is viewed in Regge phenomenology as the Pomeron ($\mathbb{P}$), with vacuum quantum numbers, being exchanged in the t-channel. Typically $\sim 10\%$ of the DIS events at HERA have a rapidity gap near the proton (forward) direction which is one of the experimental signatures of diffraction. For diffractive studies, the variables employed, in addition to Q^2, x and W, are $t = (p - p')^2$; $x_{\mathbb{P}} = \frac{q\cdot(p-p')}{q\cdot p} \approx \frac{M_X^2+Q^2-t}{W^2+Q^2+M_p^2}$, the fraction of the proton beam momentum carried by the $\mathbb{P}$; $\beta = \frac{x}{x_{\mathbb{P}}} = \frac{Q^2}{2q\cdot(p-p')} \approx \frac{Q^2}{M_X^2+Q^2-t}$, the fraction of the $\mathbb{P}$ momentum carried by the struck quark.

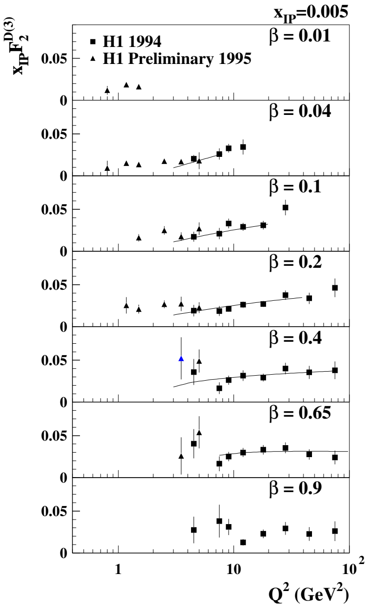

Figure 9. The diffractive structure function $x_{\mathbb{P}} F_2^{D(3)}$ as a function of Q^2 for fixed values of β. The lines correspond to the fits to the earlier H1 diffractive data.

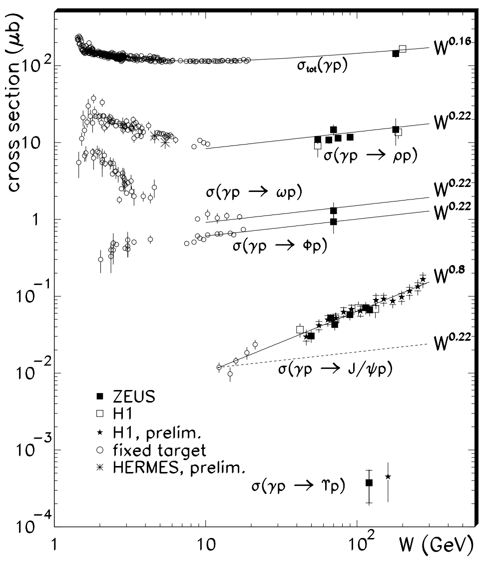

Figure 10. Photoproduction cross sections for total γp, and exclusive $\rho p, \omega p, \phi p$ and $J/\psi p$ production as a function of the γp center-of-mass energy, W.

5.1. Inclusive diffraction

$F_2^{D(4)}$ is defined by $\frac{d^4\sigma}{d\beta dQ^2 dx_{\mathbb{P}} dt} = \frac{4\pi\alpha_{em}^2}{\beta Q^4}[1 - y + \frac{y^2}{2}]F_2^{D(4)}(\beta, Q^2, x_{\mathbb{P}}, t)$. With the assumption of factorization and integration over t: $F_2^{D(3)}(\beta, Q^2, x_{\mathbb{P}}) = f_{\mathbb{P}/p}(x_{\mathbb{P}}) \cdot F_2^{\mathbb{P}}(\beta, Q^2)$. The original H1 NLO diffractive fits [11] were based on the 1994 measurements of $F_2^{D(3)}$. These fits yielded a large gluon component at high β. The fits are shown on the new H1 data [12] at high Q^2 in Fig. 9 which shows that scaling violations in diffractive F_2 (at $x_{\mathbb{P}} = 0.005$) occur at high β. Since these scaling violations persist up to $\beta \sim 0.4$ (different from F_2), DGLAP evolution requires gluons at larger β for the diffractive pdf, consistent with the gluon found in the original H1 fits [11].

5.2. Vector meson photoproduction

Vector meson production has proven to be an interesting testing ground for comparisons between data and pQCD models. In particular, studies of the transition from soft (non-perturbative) to hard (perturbative) scattering can be made by using Q^2, M_{VM}^2 and t as large scales which may be varied in a single experiment. Two of the more important features are:

1. the energy dependence of the cross section: $\sigma = a \cdot W^\delta$. One might expect that for cross sections dominated by $\mathbb{P}$ exchange (with $\alpha_{\mathbb{P}}(0) = 1.08$), $\sigma_{tot} \sim W^{0.16}$ and $\sigma_{VM} \sim W^{0.24}$. Figure 10 shows different photoproduction cross sections and that for ρ^0, ω, ϕ, $\sigma_{VM} \sim W^{0.22}$ as expected. However, J/ψ photoproduction has a steeper energy dependence than ρ^0, ω and ϕ: $\sigma_{J/\psi} \sim W^{0.8}$. This is explained in pQCD by $\sigma_{VM}^{pQCD} \sim |xg(x, Q^2)|^2$, where $xg(x, Q^2)$ is the proton gluon density – hence there appears to be a common source for the rise of F_2 and $\sigma(J/\psi)$.

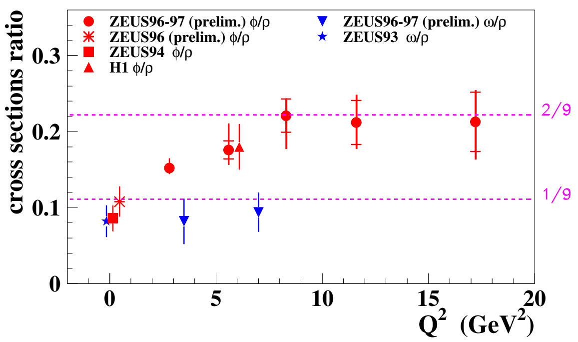

Figure 11. Ratios of the ϕ and ω cross sections to that for ρ^0 as a function of Q^2. The horizontal lines correspond to the flavor independence predictions.

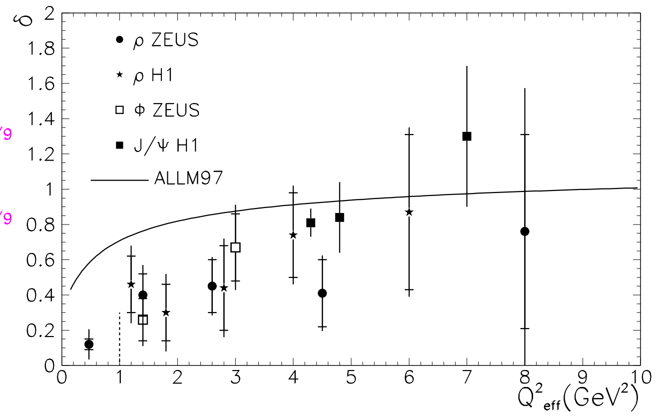

Figure 12. The value of δ obtained by fitting the W dependence of the exclusive VM cross sections to the form $\sigma \sim W^\delta$ as a function of the effective value of Q^2.

2. the ratios of the ϕ, ω and J/ψ cross sections to that for the ρ^0 as functions of Q^2 and t. From the γq coupling, one expects for flavor independence that $\rho^0 : \omega : \phi : J/\psi = 9 : 1 : 2 : 8$. For $Q^2 \gg M_{VM}^2$, pQCD predicts that $\rho^0 : \omega : \phi : J/\psi = 9 : (1 * 0.8) : (2 * 1.0) : (8 * 1.9)$. Figure 11 shows the ratios as a function of Q^2 [13] and indicates that the ratio increases from small values at $Q^2 = 0$ to values that appear consistent with those expected for flavor independence.

5.3. Vector mesons at $Q^2 > 2$ GeV^2

Fits of the ρ^0 and J/ψ cross sections as functions of W to the form $\sigma \sim W^\delta$, yields values of δ which increase with Q^2. The resulting values [14] are shown in Fig. 12 as a function of $Q^2_{eff} \approx \frac{<b^2_{\sigma L}>}{<b^2_{\rho T}>} Q^2$, a parameter which is motivated by FKS [15] based on the transverse sizes of the VM. The figure shows that δ increases with the increasing scale of the process, but may flatten at high Q^2_{eff}.

6. SUMMARY

From studies of Deep Inelastic Scattering at HERA at medium to high Q^2:

- Z^0 ($W^\pm$) contributions are observed in NC (CC) reactions in the *space−like* regime.
- One can start to distinguish the u and d pdf in a single experiment.
- NLO-pQCD fits give a good description of the data. There is no sign of a breakdown of DGLAP even at very low Q^2 (~ 0.5 GeV^2).
- The pdf's enable us to extrapolate accurately into the high Q^2 regime.
- We get a consistent gluon density from several different processes.

From studies of low Q^2 and diffraction:

- We observe a transition from the non-perturbative to the perturbative regime.
- A hard gluon component exists and DGLAP works well here also.
- When a hard scale exists (which can be Q^2, t or M_V^2), $\alpha_{\mathbb{P}}$ increases and flavor independence is approached.

REFERENCES

1. H1 Collab., Paper # 534, ICHEP98, Vancouver (1998).
2. ZEUS Collab., Paper #549, EPS99, Tampere (1999).
3. ZEUS Collab., Paper #549, EPS99, Tampere (1999).
4. ZEUS Collab., J. Breitweg et al., DESY 99-101 (1999).
5. H1 Collab., Paper #533, ICHEP98, Vancouver (1998); ZEUS Collab., J. Breitweg et al., DESY 99-059 (1999).
6. H1 Collab., C. Adloff et al., DESY 98-204 (1998).
7. ZEUS Collab., J. Breitweg et al., DESY 99-101 (1999).
8. B. W. Harris and J. Smith, Phys. Rev. D57, 2806 (1998).
9. Z. Zhang, these proceedings.
10. H1 Collab., Paper #520, ICHEP98, Vancouver (1998).
11. H1 Collab., C. Adloff et al., Zeit. f. Phys. C76, 613 (1997).
12. H1 Collab., Paper # 571, ICHEP98, Vancouver (1998).
13. ZEUS Collab., Paper #499, EPS99, Tampere, (1999).
14. H. Abramowicz, Talk at the 1999 Photon-Lepton Conf., SLAC (1999).
15. L. Frankfurt, W. Koepf and M. Strikman, Phys. Rev D57, 512 (1998).